Constraining nonstandard neutrino-quark interactions with solar, reactor, and accelerator data

F. J. Escrihuela,[1,*] O. G. Miranda,[2,†] M. A. Tórtola,[3,‡] and J. W. F. Valle[1,§]

[1]*Instituto de Física Corpuscular—C.S.I.C./Universitat de València, Campus de Paterna, Apt 22085, E-46071 València, Spain*

[2]*Departamento de Física, Centro de Investigación y de Estudios Avanzados del IPN, Apartado Postal 14-740, 07000 Mexico, DF, Mexico*

[3]*II. Institut für Theoretische Physik, Universität Hamburg, Luruper Chaussee 149, 22761 Hamburg, Germany*

(Received 17 July 2009; published 12 November 2009)

We present a reanalysis of nonstandard neutrino-down-quark interactions of electron and tau neutrinos using solar, reactor, and accelerator data. In addition updating the analysis by including new solar data from SNO phase III and Borexino, as well as new KamLAND data and solar fluxes, a key role is played in our analysis by the combination of these results with the CHARM data. The latter allows us to better constrain the axial and axial-vector electron and tau-neutrino nonstandard interaction parameters characterizing the deviations from the standard model predictions.

DOI: 10.1103/PhysRevD.80.105009 PACS numbers: 13.15.+g, 12.20.Fv, 14.60.St

I. INTRODUCTION

Current solar neutrino data [1–14], in conjunction with reactor data from the KamLAND experiment [15], show that the neutrino oscillation mechanism is the correct picture to explain the solar neutrino physics. Solar neutrino experiments are also sensitive to matter effects [16,17], and the combination of both solar and KamLAND data determines the so-called large mixing angle (LMA) solution as the correct explanation to the data. For example, the LMA solution is quite robust against possible uncertainties in solar physics, such as noise density fluctuations originated by radiative zone magnetic fields [18–25]. Likewise, the LMA solution is also stable with respect to the possible existence of sizable convective zone magnetic fields [26,27] that could induce spin-flavor neutrino conversions [28,29]. In all these cases, the KamLAND data play a crucial role in establishing that nonstandard effects can only play a subleading role [30], their amplitude being effectively constrained.

However, while constrained by the solar and KamLAND data in an important way, neutrino nonstandard interactions (NSI) still provide an important exception to the robustness of the neutrino oscillation interpretation [31,32]. Indeed, it has been found that they might even shift the solution to the so-called dark-side region of the neutrino parameter space [33].

Given the envisaged precision expected in upcoming oscillation studies [34], one needs to further scrutinize the possible role of NSI [35]. The intrinsic importance of NSI stems from the fact that they are characteristic features of theories of neutrino mass [36] and that their magnitude provides important guidance in order to distinguish the simplest high-scale seesaw models [37–41] from those seesaw scenarios based at low-scale physics, such as the inverse [42,43] or linear seesaw mechanisms [44], as well as radiative models of neutrino mass [45–47].

In this paper we reanalyze the robustness of the oscillation interpretation of the solar neutrino data in the presence of nonstandard interactions. Besides all the solar neutrino data used in our previous study [33], here we take into account new solar data from SNO phase III [11], the first real-time measurements of the solar Beryllium flux at Borexino [12], as well as the new and more precise KamLAND data [15]. We have also considered in our calculations the new solar fluxes and uncertainties from the updated standard solar model (SSM) [48]. We show explicitly that the degenerate solution in the dark-side region still remains plausible even after inclusion of these new data. Besides updating the analysis of nonstandard neutrino-down-quark interactions, we stress the key role is played by the combination of these results with the measurements of the electron-neutrino-quark cross section at the CHARM accelerator experiment. Although it is sensitive only to the interactions of electron neutrinos, when combined with solar and KamLAND data, the latter allows us to improve the determination of the tau-neutrino nonstandard axial and vector couplings.

In what follows we will focus on nonstandard interactions that can be parametrized with the effective low-energy neutral currents four-fermion operator[1]:

$$\mathcal{L}_{\mathrm{NSI}} = -\varepsilon_{\alpha\beta}^{fP} 2\sqrt{2} G_F (\bar{\nu}_\alpha \gamma_\mu L \nu_\beta)(\bar{f}\gamma^\mu P f), \qquad (1)$$

where $P = L, R$ and f is a first generation fermion: e, u, d. The coefficients $\varepsilon_{\alpha\beta}^{fP}$ denote the strength of the NSI between the neutrinos of flavors α and β and the P-handed component of the fermion f. For definiteness, we take for f

*franesfe@alumni.uv.es
†Omar.Miranda@fis.cinvestav.mx
‡mariam.tortola@desy.de
§valle@ific.uv.es; http://ahep.uv.es/

[1]A recent study of charged current nonstandard interactions has been given in Ref. [49].

the down-type quark. However, one can also consider the presence of NSI with electrons and up and down quarks simultaneously. Current and expected limits for the case of NSI with electrons have been reported in the literature [50–52]. Here we confine ourselves to NSI couplings involving only electron and tau neutrinos. This approximation is in principle justified in view of the somewhat stronger constraints on ν_μ interactions; for a discussion see Refs. [53–55].

Nonstandard interactions may in principle affect neutrino propagation properties in matter as well as detection cross sections and in certain cases they can also modify the assumed initial fluxes.[2] NSI effects in neutrino propagation affect the analysis of data from solar neutrino experiments and to some extent also KamLAND, through the vectorial NSI couplings $\varepsilon^{dV}_{\alpha\beta} = \varepsilon^{dL}_{\alpha\beta} + \varepsilon^{dR}_{\alpha\beta}$. On the other hand, detection shows sensitivity also to the axial NSI couplings $\varepsilon^{dA}_{\alpha\beta} = \varepsilon^{dL}_{\alpha\beta} - \varepsilon^{dR}_{\alpha\beta}$ in the SNO experiment. These points will be analyzed in detail in Sec. II, after a brief discussion of the experimental data included in our study. In Sec. III we will focus on the study of the nonuniversal nonstandard interactions, combining the results of the CHARM experiment together with our solar analysis in order to obtain a new constraint for the tau-neutrino nonstandard interaction with a *d*-type quark. Finally we will conclude in Sec. IV.

II. SENSITIVITY OF SOLAR AND KAMLAND DATA TO NSI

Here we will adopt the simplest approximate two-neutrino picture, which is justified in view of the stringent limit on θ_{13} [56] that follows mainly from reactor neutrino experiments [57].

A. Data

In this section we will describe the input data required to analyze the sensitivity of solar and KamLAND neutrino data to the presence of NSI. This will include not only the experimental data samples by all the detectors considered, but also the theoretical predictions required to simulate the solar neutrino production prescribed by the SSM.

Concerning the solar neutrino data, we have included in our analysis the most recent results from the radiochemical experiments Homestake [1], SAGE [2], and GALLEX/GNO [3,4], the zenith-spectra data set from Super-Kamiokande I [5,6], as well as the results from the two first phases of the SNO experiment [7–10]. The main updates with respect to our previous work [33] are the inclusion of the data from the third phase of the SNO experiment [11], where ^{3}He proportional counters have been used to measure the neutral current (NC) component of the solar neutrino flux, and the latest measurement of the ^{7}Be solar neutrino rate performed by the Borexino Collaboration [12,13].

In our analysis we use the solar neutrino fluxes and uncertainties given by the latest version of the SSM [48]. The latter provides an improved determination of the neutrino flux uncertainties, mainly thanks to the improved accuracy on the ^{3}He-^{4}He cross section measurement and to the reduced systematic uncertainties in the determination of the surface composition of the Sun. In Ref. [48] two different solar model calculations are presented, corresponding to two different measurements of the solar metal abundances. For our analysis we have chosen the model corresponding to a higher solar metallicity, BPS08(GS), although we have checked that the use of the lower metallicity model BPS08(AGS) does not change our results substantially.

The KamLAND experiment observes the disappearance of reactor antineutrinos over an average distance of 180 km. Given that, on their way to the detector, reactor neutrinos can only traverse the most superficial layers of the Earth, and the resulting Earth matter effects are almost negligible. The same applies also to the nonstandard interactions we are considering. However, for consistency with our analysis of solar neutrino data, in our simulation of the KamLAND experiment, we have included the effect of NSI over the antineutrino propagation. In particular, we have considered that neutrinos travel through a layer of constant matter density equal to the terrestrial crust density ($\sim 2.6\ \mathrm{g\,cm^{-3}}$). Here we have used the latest data release from the KamLAND reactor experiment [15], with a total exposure of 2881 ton yr, which brings in a big statistical improvement with respect to the previous data reported by the collaboration [58]. We have restricted our analysis to the energy range above 2.6 MeV where the contributions from geo-neutrinos are less important. As we will see in the next section, the inclusion of the new KamLAND data will be very important for the improvement of the results, given the good precision achieved in the determination of the oscillation neutrino parameters.

B. Effects in neutrino propagation

We first reanalyze the determination of the oscillation parameters in the presence of nonstandard interactions. The Hamiltonian describing solar neutrino evolution in the presence of NSI contains, in addition to the standard oscillation term,

$$\begin{pmatrix} -\frac{\Delta m^2}{4E}\cos 2\theta + \sqrt{2}G_F N_e & \frac{\Delta m^2}{4E}\sin 2\theta \\ \frac{\Delta m^2}{4E}\sin 2\theta & \frac{\Delta m^2}{4E}\cos 2\theta \end{pmatrix}, \tag{2}$$

a term H_{NSI} accounting for an effective potential induced by the NSI with matter, which may be written as

$$H_{\mathrm{NSI}} = \sqrt{2}G_F N_d \begin{pmatrix} 0 & \varepsilon \\ \varepsilon & \varepsilon' \end{pmatrix}. \tag{3}$$

[2]We assume a class of models of neutrino mass where NSI leave the solar and reactor neutrino fluxes unaffected.

Here ε and ε' are two effective parameters that, according to the current bounds discussed above ($\varepsilon^{fP}_{\alpha\mu} \sim 0$), are related with the vectorial couplings which affect the neutrino propagation by[3]:

$$\varepsilon = -\sin\theta_{23}\varepsilon^{dV}_{e\tau}, \qquad \varepsilon' = \sin^2\theta_{23}\varepsilon^{dV}_{\tau\tau} - \varepsilon^{dV}_{ee}. \tag{4}$$

The quantity N_d in Eq. (3) is the number density of the down-type quark along the neutrino path, and θ_{23} is the atmospheric neutrino mixing angle.

From Eqs. (2) and (3) one sees that the solar neutrino mixing angle in the presence of nonstandard interactions is given by the following expression:

$$\cos2\theta_m = \frac{\Delta m^2\cos2\theta - 2\sqrt{2}EG_F(N_e - \varepsilon' N_d)}{[\Delta m^2]_{\text{matter}}}, \tag{5}$$

where

$$[\Delta m^2]_{\text{matter}} = [\Delta m^2\cos2\theta - 2\sqrt{2}EG_F(Ne - \varepsilon' N_d)]^2 + [\Delta m^2\sin2\theta + 4\sqrt{2}\varepsilon EG_F N_d]^2. \tag{6}$$

Therefore, and as discussed in Ref. [33], there exists a degeneracy between the nonuniversal coupling ε' and the neutrino mixing angle θ, which makes it possible to explain the solar neutrino data for values of the vacuum mixing angle in the dark side ($\theta > \pi/4$), for large enough values of ε':

$$\varepsilon' > \frac{2\sqrt{2}EG_F N_e + \Delta m^2|\cos2\theta|}{2\sqrt{2}EG_F N_d}. \tag{7}$$

For instance, for the typical values of the solar neutrino energies and matter densities one has $\varepsilon' \gtrsim 0.6$. Indeed, as we showed in [33], the effect of NSI on solar neutrino propagation implies the presence of an additional LMA-D solution whose status we now reanalyze in the light of new data.

We now turn to the combined solar + KamLAND analysis. Following the considerations above, we performed a new analysis of all the solar neutrino data discussed in Sec. II A combined with the recent KamLAND result [15]. The main result is shown in Fig. 1. There, we plot the allowed regions (90%, 95%, and 99% C.L.) in the solar neutrino oscillation parameter space ($\sin^2\theta_{\text{SOL}}$, Δm^2_{SOL}) obtained in the analysis of solar and solar + KamLAND neutrino data, after marginalizing over the NSI parameters in our four-dimensional χ^2 analysis: $\chi^2(\sin^2\theta_{\text{SOL}}, \Delta m^2_{\text{SOL}}, \varepsilon, \varepsilon')$. The $\Delta\chi^2$ profiles as a function of each parameter are also shown. One can see that the region in the so-called dark side of the neutrino parameters [33] remains even after the inclusion of the new data. Note however that its status is somewhat worse than previously shown in Ref. [33]. In contrast, as seen in the figure, the other solutions LMA-0 and LMA-II [33] which were present before have disappeared as a result of the new KamLAND data that now provide a very precise measurement of Δm^2.

In order to better understand the results obtained, we plot in Fig. 2 the neutrino survival probabilities for different reference points. First we have considered the global best fit point from the combined solar + KamLAND analysis, labeled as "global best fit" in the figure, with the following parameter values: ($\sin^2\theta_{\text{SOL}}$, Δm^2_{SOL}, ε, ε') = (0.32, 7.9×10^{-5} eV^2, -0.15, -0.10). We have also considered the best fit point in the absence of NSI: (0.30, 7.9×10^{-5} eV^2, 0.00, 0.00), labeled as "BF without NSI," and allowed with a $\Delta\chi^2 = 2.7$, and finally the best fit point in the "dark side" of the oscillation parameters (labeled as "BF dark side") with (0.70, 7.9×10^{-5} eV^2, -0.15, 0.95) and $\Delta\chi^2 = 2.9$. As we see all points are in perfect agreement with the low energy (pp and ^{7}Be) measurements. Concerning the most energetic boron neutrinos, where matter effects are more important, and as a result there is a higher NSI sensitivity of the corresponding profiles, the presence of NSI provides a slightly better agreement with the data than the standard one without NSI, mainly thanks to the flatter spectrum predicted above 5 MeV. The dark-side solution also gives predictions for the survival probability of boron neutrinos which are compatible with the experimental results. From the different predictions obtained for these 3 reference points above a few MeV, one sees that this region could be crucial in order to break the degeneracy among the various solutions. Therefore, a better measurement of the boron neutrino flux with a lower threshold (like the ones expected from Super-K-III and SNO [60,61]) will be of great help. On the other hand, a very precise measurement of the pep and beryllium neutrino fluxes may also contribute to lift the degeneracy between the standard and dark-side solutions.

By analyzing the goodness of the neutrino oscillation solutions in the presence of NSI, one can also constrain the NSI parameters ε and ε'. In order to do this we first marginalize our 4-parameter χ^2 analysis with respect to the remaining three-neutrino parameters. The results are shown in Fig. 3. One can see that the new data allow us to constraint ε, the flavor-changing parameter, while for the flavor-conserving case there is still room for relatively large values of ε' that correspond to the solution on the dark side of the neutrino oscillation parameters. These are the bounds we obtained at the 90% C.L.:

$$-0.41 < \varepsilon < 0.06, \tag{8}$$

$$-0.50 < \varepsilon' < 0.19 \quad \text{and} \quad 0.89 < \varepsilon' < 0.99. \tag{9}$$

The above limits are in good agreement with the forecast made in Fig. 3 of [33], assuming the best possible determination of the neutrino mixing parameters due to KamLAND. In fact, they are even a bit better than expected

[3]For the derivation of the effective couplings in the general three-neutrino framework, see Ref. [59].

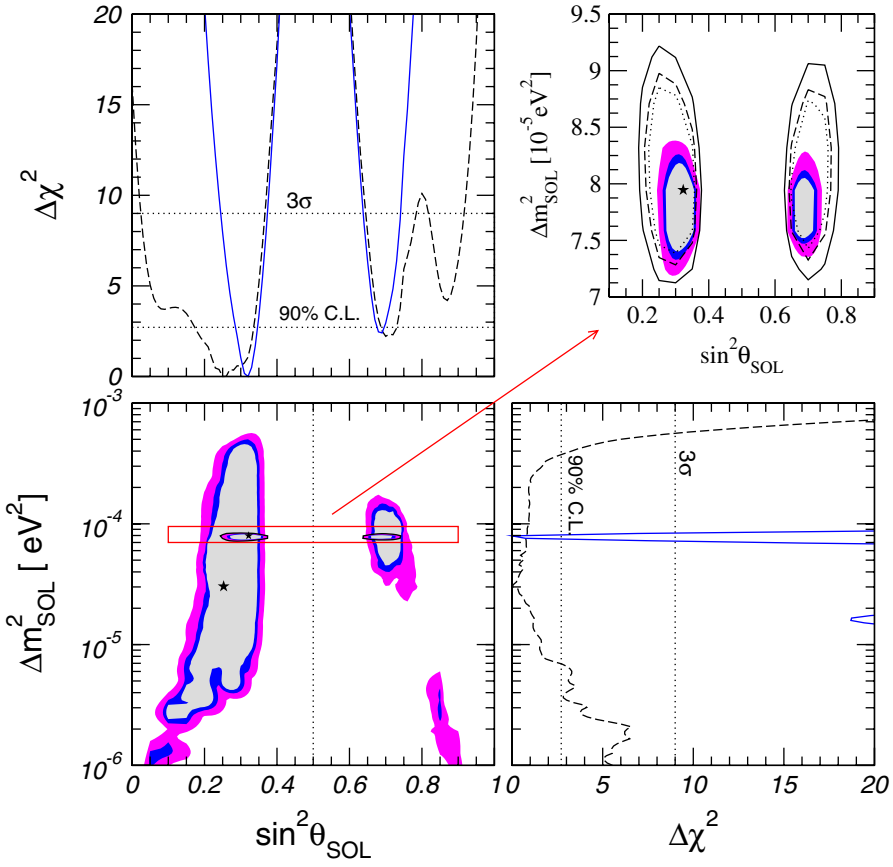

FIG. 1 (color online). The bottom left panel indicates 90%, 95%, and 99% C.L. allowed regions from the solar and solar + KamLAND combined analysis, the result of which is presented as a zoom in the top right panel, where the shaded regions show the result of the current analysis while the lines indicate the earlier regions [33] for comparison. One sees that the dark-side solution is still allowed in the presence of nonstandard interactions. The other two panels indicate the corresponding χ^2 projections. In all cases, we marginalize over the NSI parameters ε and ε'.

from the improvement of KamLAND data only. The reason for this is the subsequent improvement of solar data, which slightly improved their sensitivity to the nonstandard interactions.

For the flavor-changing effective coupling ε, one can use the first expression in Eq. (4) to translate the bound obtained in Eq. (8) into a limit over the vectorial coupling $\varepsilon^{dV}_{e\tau}$:

$$-0.08 < \varepsilon^{dV}_{e\tau} < 0.58 \qquad (90\%\ \text{C.L.}), \qquad (10)$$

where we have used the best fit value for the atmospheric mixing angle [56]. So far, the strongest limit on this parameter is $|\varepsilon^{dV}_{e\tau}| < 0.5$ [53]. From our analysis, we see that solar neutrino data are not only sensitive to the sign of this coupling but also we have improved the lower bound.

C. Effects in neutrino detection

The presence of nonstandard interactions can also affect the detection processes at some experiments. In particular, the cross section for the neutral current detection reaction at SNO

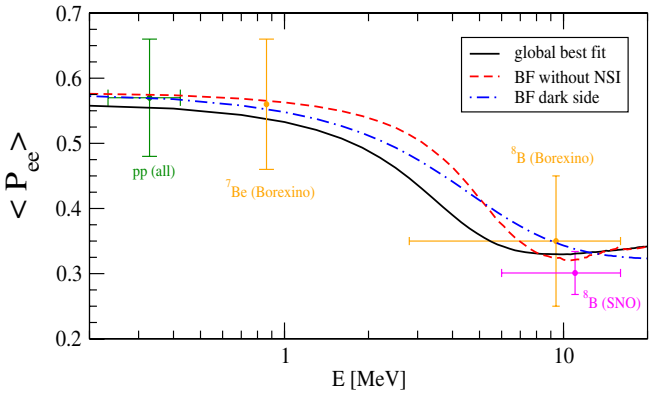

FIG. 2 (color online). Neutrino survival probabilities averaged over the ^{8}B neutrino production region for three reference points (see text for details). Lines are compared with the experimental rates for the pp neutrino flux (from the combination of all solar experiments), the 0.862 MeV ^{7}Be line (from Borexino) and two estimated values of the ^{8}B neutrino flux from Borexino and SNO (third phase). Here, vertical error bars correspond to the experimental errors, while the horizontal ones indicate the energy range observed at the experiment.

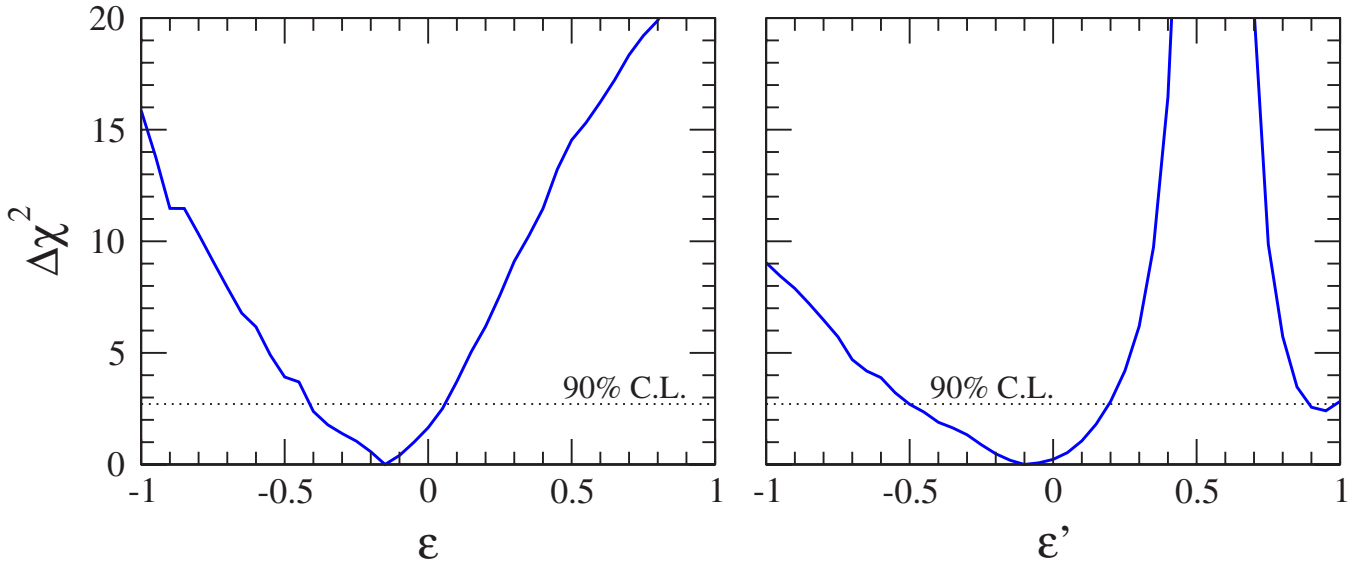

FIG. 3 (color online). Bounds on ε and ε' from the combined analysis of solar + KamLAND neutrino data. One sees that the ε parameter is now constrained to only one region while for the case of ε' there are two possible regions, one corresponding to the standard light-side solution and the other one (less favored) to the so-called dark-side region.

$$\nu + d \rightarrow \nu + p + n \tag{11}$$

is proportional to g_A^2, where g_A is the coupling of the neutrino current to the axial isovector hadronic current [62]. Therefore, the presence of an axial nonstandard coupling would give rise to an extra contribution to the NC signal at the SNO experiment. This nonstandard contribution can be parametrized in the following way [53]:

$$\phi_{\mathrm{NC}} \sim f_B(1 + 2\varepsilon_A), \tag{12}$$

where terms of order ε_A^2 have been neglected. Here f_B denotes the boron neutrino flux, and the effective axial coupling ε_A is defined as in [53]:

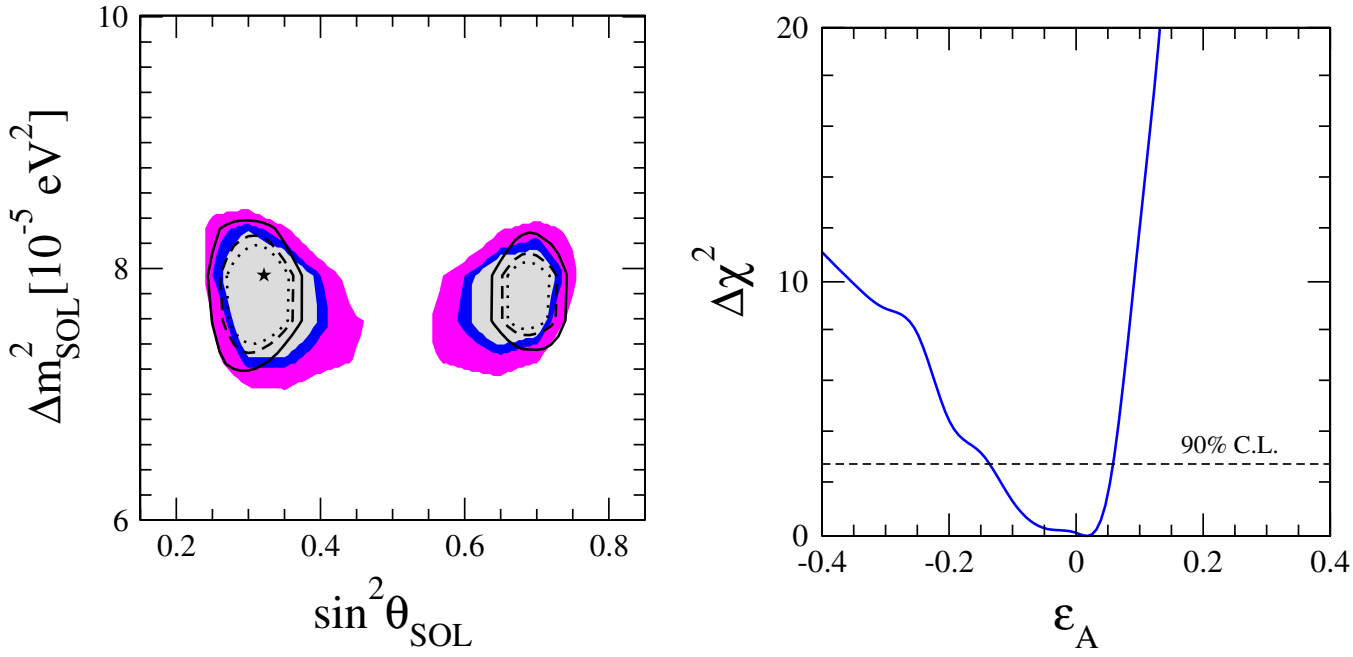

FIG. 4 (color online). The shaded regions in the left panel show the updated analysis of all solar neutrino data combined with recent KamLAND results in the presence of the axial NSI coupling. The lines show, for comparison, the updated regions obtained only with the vector NSI couplings. We show in the right panel the χ^2 profile with respect to the axial NSI parameter obtained using all solar neutrino data combined with KamLAND. One sees how the data prefer $\varepsilon_A \sim 0$.

$$\varepsilon_A = -\sum_{\alpha=e,\mu,\tau} \langle P_{e\alpha}\rangle_{\rm NC}\varepsilon^{dA}_{\alpha\alpha}, \tag{13}$$

once the nonstandard axial couplings with up-type quarks are set to zero. Note that $\varepsilon^{dA}_{\alpha\alpha} = \varepsilon^{dL}_{\alpha\alpha} - \varepsilon^{dR}_{\alpha\alpha}$, denoting the couplings entering in the effective Lagrangian shown in Eq. (1). Thus, ε_A is independent of the effective couplings ε and ε' defined in Eq. (4). So far we have assumed in our analysis that $\varepsilon_A = 0$. This assumption is well justified due to the good agreement between the SNO NC measurement: $\phi^{\rm SNO}_{\rm NC} = 5.54^{+0.33}_{-0.31}({\rm stat})^{+0.36}_{-0.34}({\rm syst}) \times 10^6\ {\rm cm}^{-2}\,{\rm s}^{-1}$ [11] and the SSM prediction for the boron flux $f_B = 5.94 \pm 0.65 \times 10^6\ {\rm cm}^{-2}\,{\rm s}^{-1}$ [48]. However, we now relax this assumption by including the effect of the new parameter ε_A.

The results obtained in a generalized 5-parameter analysis which takes into account the presence of a nonzero axial component of the NSI are summarized in Fig. 4. In the left panel we compare the allowed regions at 90%, 95%, and 99% C.L. obtained in the full 5-parameter analysis (filled/colored regions) with the ones obtained in the previous section, neglecting the effect of the axial NSI couplings (hollow lines). One sees that both analyses are consistent, though, as expected, the inclusion of the axial parameter in the analysis somewhat extends the allowed region. In the right panel we show the $\Delta\chi^2$ profile as a function of the effective axial coupling ε_A. There, one sees that the neutrino data clearly prefer $\varepsilon_A \sim 0$, thanks to the good agreement between the predicted boron neutrino flux and the NC observations at SNO, as stated above. We obtain the following allowed range at 90% C.L.:

$$-0.14 < \varepsilon_A < 0.06. \tag{14}$$

Using Eq. (13), the above bound on the effective axial coupling ε_A can be translated into individual bounds on the NSI parameters $\varepsilon^{dA}_{\alpha\alpha}$. Since we are neglecting the nonstandard interactions of the muon neutrino, this formula depends only on the probabilities $\langle P_{ee}\rangle_{\rm NC}$, $\langle P_{e\tau}\rangle_{\rm NC}$ and on the NSI couplings ε^{dA}_{ee} and $\varepsilon^{dA}_{e\tau}$. From the recent values for the average probabilities reported by SNO [11]:

$$\langle P_{ee}\rangle_{\rm NC} = 0.30 \pm 0.03, \qquad \langle P_{e\tau}\rangle_{\rm NC} = 0.35 \pm 0.02, \tag{15}$$

one gets an allowed region in the parameter space $(\varepsilon^{dA}_{ee}, \varepsilon^{dA}_{e\tau})$, represented (at the 90% C.L.) as a diagonal band in Fig. 6 in the next section. There, it will be used combined with neutrino laboratory data to obtain improved constraints on the neutrino NSI couplings.

III. CONSTRAINTS ON NONUNIVERSAL NSI

In addition to the solar + KamLAND data, laboratory experiments measuring neutrino-nucleon scattering show sensitivity to neutrino nonstandard interactions on d-type quarks. In particular, here we will combine the results of the accelerator experiment CHARM together with the ones in Sec. II in order to obtain stronger constraints on the NSI parameters. Given the sensitivity of the considered experiments to different NSI parameters, we have been forced to simplify the analyses reducing the number of parameters by focusing on the flavor-conserving nonuniversal nonstandard couplings. Within this approximation, the parameters relevant for each experiment are shown in Table I.

TABLE I. Sensitivity of neutrino experiments to flavor-conserving NSI parameters.

Data	ε^{dV}_{ee}	$\varepsilon^{dV}_{\tau\tau}$	ε^{dA}_{ee}	$\varepsilon^{dA}_{\tau\tau}$
Solar propagation	√	√		
Solar NC detection			√	√
KamLAND propagation	√	√		
CHARM detection	√		√	

A. CHARM

We now turn to the analysis of the CHARM data. CHARM was an accelerator experiment measuring the ratio of the neutral current to the charge current cross section for electron (anti)neutrinos off quarks. We have used the results reported by the CHARM experiment for the $\nu_e q \to \nu q$ cross section. In particular, the experiment measured the relation [63],

$$R^e = \frac{\sigma(\nu_e N \to \nu_e X) + \sigma(\bar\nu_e N \to \bar\nu X)}{\sigma(\nu_e N \to e X) + \sigma(\bar\nu_e N \to \bar e X)} = (\tilde g_{Le})^2 + (\tilde g_{Re})^2 = 0.406 \pm 0.140. \tag{16}$$

The most general expression for $(\tilde g_{L,Re})^2$ including all types of NSI parameters is given by

$$(\tilde g_{Le})^2 = (g^u_L + \varepsilon^{uL}_{ee})^2 + \sum_{\alpha\neq e}|\varepsilon^{uL}_{\alpha e}|^2 + (g^d_L + \varepsilon^{dL}_{ee})^2 + \sum_{\alpha\neq e}|\varepsilon^{dL}_{\alpha e}|, \tag{17}$$

$$(\tilde g_{Re})^2 = (g^u_R + \varepsilon^{uR}_{ee})^2 + \sum_{\alpha\neq e}|\varepsilon^{uR}_{\alpha e}|^2 + (g^d_R + \varepsilon^{dR}_{ee})^2 + \sum_{\alpha\neq e}|\varepsilon^{dR}_{\alpha e}|. \tag{18}$$

Here we are interested in the flavor-conserving d-type quark interaction. Then, we will neglect all flavor-changing nonstandard contributions, implying that $\varepsilon^{qL}_{\alpha e} = 0$, as well as nonstandard couplings to the u-type quark, so that $\varepsilon^{uP}_{ee} = 0$. In this case our simplified expression for Eqs. (17) and (18) would be

$$(\tilde g_{Le})^2 = (g^u_L)^2 + (g^d_L + \tfrac{1}{2}(\varepsilon^{dV}_{ee} + \varepsilon^{dA}_{ee}))^2, \tag{19}$$

$$(\tilde g_{Re})^2 = (g^u_R)^2 + (g^d_R + \tfrac{1}{2}(\varepsilon^{dV}_{ee} - \varepsilon^{dA}_{ee}))^2. \tag{20}$$

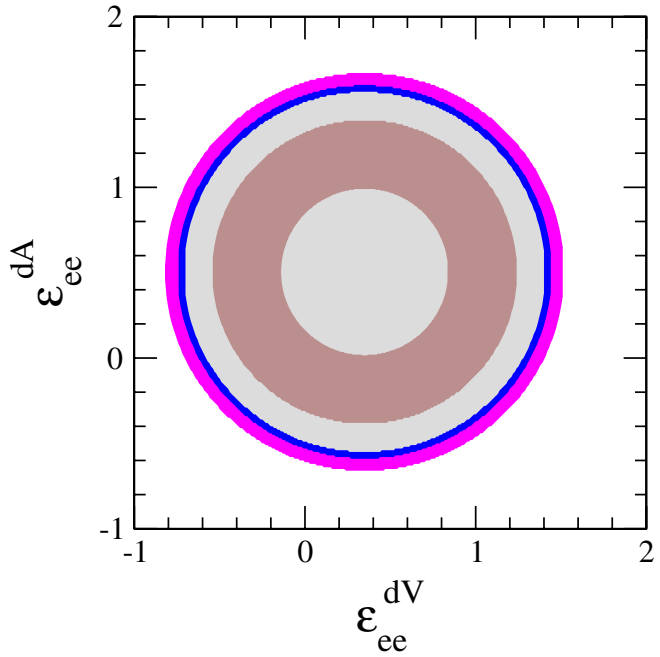

FIG. 5 (color online). Constraints at 68%, 90%, 95%, and 99% C.L. on the neutrino NSI couplings ε_{ee}^{dV} and ε_{ee}^{dA} from CHARM data.

Then, we can compute the χ^2 for the CHARM data:

$$\chi^2 = \frac{(R^e - R^{\text{theo}}(\varepsilon_{ee}^{dV}, \varepsilon_{ee}^{dA}))^2}{(\sigma_R^e)^2}, \tag{21}$$

where R^e and σ_R^e are defined by the result given in Eq. (15).

The constraints in the $(\varepsilon_{ee}^{dV}, \varepsilon_{ee}^{dA})$ plane at 68%, 90%, 95%, and 99% C.L. obtained from this analysis are shown in Fig. 5.

B. Combined analysis

In the previous sections we discussed the sensitivity of solar experiments, KamLAND and CHARM, to the nonstandard interactions separately. In this section we exploit the complementarity of the information we can get from the different experiments by combining CHARM data with our previous results from the analysis of the solar and KamLAND data. This enables us to obtain stronger constraints on the NSI couplings.

The regions for the vector (left panel) and axial-vector (right panel) NSI couplings allowed by the global analysis are given in Fig. 6, where they are also compared with the constraints coming only from the CHARM data and that from the solar + KamLAND data. First, the bounds obtained from the analysis of CHARM data and shown in Fig. 5 have been translated into two independent bounds on ε_{ee}^{dV} and ε_{ee}^{dA} (see vertical bands in Fig. 6). The regions allowed by the solar + KamLAND combination (diagonal bands in the figure) have been derived from the bounds on the nonuniversal nonstandard neutrino interactions obtained in Sec. II. In particular, the limits on the vectorial couplings ε_{ee}^{dV} and $\varepsilon_{\tau\tau}^{dV}$ come from the allowed values for the effective coupling ε' in Eq. (8), after using the definition of ε' of Eq. (4) and the 1σ allowed region for the atmospheric mixing angle θ_{23} [56]. Note the existence of two allowed islands in correspondence with the two allowed regions of neutrino oscillation parameters in the presence of NSI (see upper-right panel of Fig. 1). The

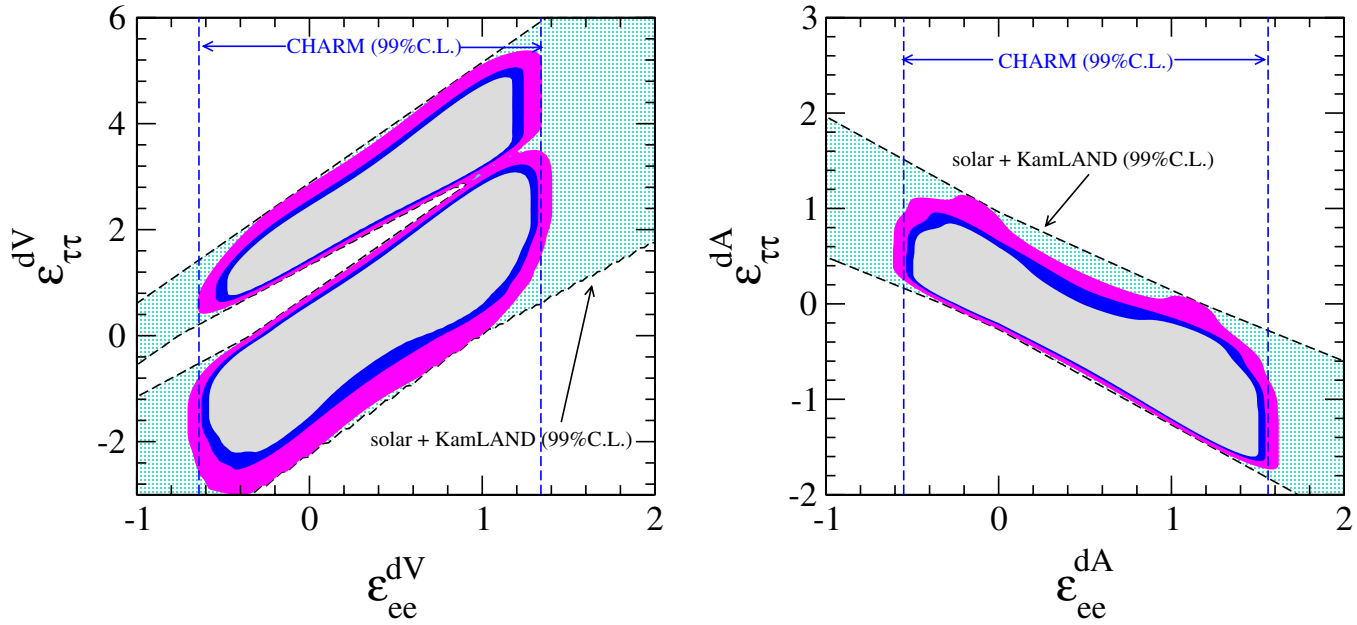

FIG. 6 (color online). Constraints on the vector (left panel) and axial-vector (right panel) NSI couplings from our global analysis at 90%, 95%, and 99% C.L., and from the separate solar + KamLAND and CHARM data sets (dashed lines).

TABLE II. New constraints on the vectorial and axial NSI couplings at 90% C.L. obtained from the analysis of CHARM data alone and from our global analysis combining CHARM with solar and KamLAND results.

	Vectorial couplings	
Global	$-0.5 < \varepsilon_{ee}^{dV} < 1.2$	$-1.8 < \varepsilon_{\tau\tau}^{dV} < 4.4$
	One parameter at a time	
CHARM	$-0.5 < \varepsilon_{ee}^{dV} < 1.2$	
Global	$-0.2 < \varepsilon_{ee}^{dV} < 0.5$	$-1.1 < \varepsilon_{\tau\tau}^{dV} < 0.4$ & $1.6 < \varepsilon_{\tau\tau}^{dV} < 2.2$
	Axial couplings	
Global	$-0.4 < \varepsilon_{ee}^{dA} < 1.4$	$-1.5 < \varepsilon_{\tau\tau}^{dA} < 0.7$
	One parameter at a time	
CHARM	$-0.4 < \varepsilon_{ee}^{dA} < 1.4$	
Global	$-0.2 < \varepsilon_{ee}^{dA} < 0.3$	$-0.2 < \varepsilon_{\tau\tau}^{dA} < 0.4$

lower one corresponds to the usual LMA solution, while the upper island comes from the solution in the dark side. On the other hand, using the average probabilities in Eq. (15) we have reanalyzed the results obtained for the effective axial coupling ε_A in Eq. (14). This results in a constraint for the axial couplings ε_{ee}^{dA} and $\varepsilon_{\tau\tau}^{dA}$. From the two panels of Fig. 6 one sees that, as expected, there is a degeneracy in the determination of the two vectorial and axial parameters from solar and KamLAND data only. After the combination with CHARM we break this degeneracy and obtain the allowed regions shown in color at Fig. 6.

In Table II we quote the 90% C.L. allowed intervals for the couplings ε_{ee}^{dV}, $\varepsilon_{\tau\tau}^{dV}$, ε_{ee}^{dA}, and $\varepsilon_{\tau\tau}^{dA}$ arising from the combined analysis, as taken directly from Fig. 6. In order to compare with previous bounds obtained in a one-parameter-at-a-time analysis [53], we also present the results obtained following that approach in our analysis of CHARM data alone and in the global analysis including solar and KamLAND data as well. In this case, we see how the combination with solar and KamLAND data improves significantly the existing bounds on the electron-neutrino NSI couplings, obtained using CHARM data only [53]. Now, concerning the tau-neutrino NSI couplings, we have improved the existing bounds derived from the invisible decay width measurement of the Z from LEP data: $|\varepsilon_{\tau\tau}^{dV}| < 2.7$, $|\varepsilon_{\tau\tau}^{dA}| < 1.8$ [53].

IV. CONCLUSIONS

We have updated the solar neutrino analysis for the case of NSI of neutrinos with a d-type quark by including new solar data from SNO phase III and Borexino, as well as new KamLAND data and updated solar fluxes. We have found that the additional dark side of neutrino parameter space found in Ref. [33] still survives, while the previous LMA-0 and LMA-II which were present before have now disappeared as a result of the new data. The issue arises of how to lift this degeneracy in future studies. First we note that, since KamLAND is basically insensitive to matter effects, it will not help in resolving the degeneracy, as explicitly verified in Fig. 3 of Ref. [33]. Next comes improved solar neutrino data. The form of the expected neutrino survival probability shown in Fig. 2 suggests that the best region to discriminate the degenerate solution from the normal one is the intermediate energy solar neutrino region, where the relevant experiments are Borexino [12–14] and KamLAND solar [64], as well as the low energy threshold analysis expected from Super-K-III and SNO [60,61].

Further information relevant to lift the degeneracy may come from atmospheric and laboratory data. Indeed the LMA-D solution induced by nonstandard interactions of neutrinos with quarks may become inconsistent with atmospheric and laboratory data [33,65]. As noted in Ref. [33], currently it is not. Should the situation change with improved data we note that still the degeneracy will not disappear since the NSI couplings may affect not only down-type quark species but also up-type quarks and/or electrons. The analysis in this case would introduce new parameters. Therefore, we conclude that the neutrino oscillation interpretation of solar neutrino data is still fragile with respect to the presence of nonstandard interactions.

In summary, we have studied the limits on the nonstandard interaction couplings ε_{ee}^{dV}, $\varepsilon_{e\tau}^{dV}$, $\varepsilon_{\tau\tau}^{dV}$, ε_{ee}^{dA}, and $\varepsilon_{\tau\tau}^{dA}$ from present neutrino data. Thanks to the combination of solar and KamLAD neutrino data with the results from the CHARM experiment, we have given improved bounds on the vector and axial NSI couplings involving electron and tau-neutrino interactions on down-type quarks.

ACKNOWLEDGMENTS

This work was supported by Spanish Grants No. FPA2008-00319/FPA and No. PROMETEO/2009/091. O. G. M. was supported by CONACyT-Mexico and SNI. M. A. T. was supported by the DFG (Germany) under Grant No. SFB-676. F. J. E. thanks Cinvestav for hospitality where part of this work was performed.

[1] B. T. Cleveland *et al.*, Astrophys. J. **496**, 505 (1998).
[2] J. N. Abdurashitov *et al.* (SAGE Collaboration), Phys. Rev. C **80**, 015807 (2009).
[3] M. Altmann *et al.* (GNO Collaboration), Phys. Lett. B **616**, 174 (2005).
[4] F. Kaether, Heidelberg, 2007, http://www.ub.uni-heidelberg.de/archiv/7501/.
[5] S. Fukuda *et al.* (Super-Kamiokande Collaboration), Phys. Lett. B **539**, 179 (2002).
[6] J. Hosaka *et al.* (Super-Kamkiokande Collaboration), Phys. Rev. D **73**, 112001 (2006).
[7] Q. R. Ahmad *et al.* (SNO Collaboration), Phys. Rev. Lett. **89**, 011301 (2002).
[8] Q. R. Ahmad *et al.* (SNO Collaboration), Phys. Rev. Lett. **89**, 011302 (2002).
[9] S. N. Ahmed *et al.* (SNO Collaboration), Phys. Rev. Lett. **92**, 181301 (2004).
[10] B. Aharmim *et al.* (SNO Collaboration), Phys. Rev. C **72**, 055502 (2005).
[11] B. Aharmim *et al.* (SNO Collaboration), Phys. Rev. Lett. **101**, 111301 (2008).
[12] C. Arpesella *et al.* (The Borexino Collaboration), Phys. Rev. Lett. **101**, 091302 (2008).
[13] C. Galbiati *et al.*, J. Phys. Conf. Ser. **136**, 022001 (2008).
[14] G. Bellini *et al.* (Borexino Collaboration), arXiv: 0808.2868.
[15] S. Abe *et al.* (KamLAND Collaboration), Phys. Rev. Lett. **100**, 221803 (2008).
[16] L. Wolfenstein, Phys. Rev. D **17**, 2369 (1978).
[17] S. P. Mikheev and A. Y. Smirnov, Sov. J. Nucl. Phys. **42**, 913 (1985).
[18] A. Schaefer and S. E. Koonin, Phys. Lett. B **185**, 417 (1987).
[19] P. I. Krastev and A. Y. Smirnov, Mod. Phys. Lett. A **6**, 1001 (1991).
[20] F. N. Loreti and A. B. Balantekin, Phys. Rev. D **50**, 4762 (1994).
[21] H. Nunokawa, A. Rossi, V. B. Semikoz, and J. W. F. Valle, Nucl. Phys. **B472**, 495 (1996).
[22] C. P. Burgess, N. S. Dzhalilov, T. I. Rashba, V. B. Semikoz, and J. W. F. Valle, Mon. Not. R. Astron. Soc. **348**, 609 (2004).
[23] C. Burgess *et al.*, Astrophys. J. **588**, L65 (2003).
[24] C. P. Burgess *et al.*, J. Cosmol. Astropart. Phys. 01 (2004) 007.
[25] G. L. Fogli, E. Lisi, A. Marrone, D. Montanino, and A. Palazzo, Phys. Rev. D **76**, 033006 (2007).
[26] O. G. Miranda *et al.*, Nucl. Phys. **B595**, 360 (2001).
[27] O. G. Miranda, T. I. Rashba, A. I. Rez, and J. W. F. Valle, Phys. Rev. Lett. **93**, 051304 (2004).
[28] J. Schechter and J. W. F. Valle, Phys. Rev. D **24**, 1883 (1981); **25**, 283(E) (1982).
[29] E. K. Akhmedov, Phys. Lett. B **213**, 64 (1988).
[30] S. Pakvasa and J. W. F. Valle, in *Proceedings of the Indian National Academy of Sciences on Neutrinos*, edited by D. Indumathi, M. V. N. Murthy, and G. Rajasekaran, 2004, Vol. 70A, No. 1, pp. 189–222.
[31] A. Friedland, C. Lunardini, and C. Pena-Garay, Phys. Lett. B **594**, 347 (2004).
[32] M. M. Guzzo, P. C. de Holanda, and O. L. G. Peres, Phys. Lett. B **591**, 1 (2004).
[33] O. G. Miranda, M. A. Tortola, and J. W. F. Valle, J. High Energy Phys. 10 (2006) 008.
[34] A. Bandyopadhyay *et al.* (ISS Physics Working Group), Rep. Prog. Phys. **72**, 106201 (2009).
[35] H. Nunokawa, S. J. Parke, and J. W. F. Valle, Prog. Part. Nucl. Phys. **60**, 338 (2008.
[36] J. W. F. Valle, J. Phys. Conf. Ser. **53**, 473 (2006), review based on lectures at the Corfu Summer Institute on Elementary Particle Physics in September 2005.
[37] M. Gell-Mann, P. Ramond, and R. Slansky, CERN Report No. 80-0576, 1979.
[38] T. Yanagida, KEK Lectures, edited by O. Sawada and A. Sugamoto, KEK, 1979.
[39] R. N. Mohapatra and G. Senjanovic, Phys. Rev. Lett. **44**, 91 (1980).
[40] J. Schechter and J. W. F. Valle, Phys. Rev. D **22**, 2227 (1980).
[41] J. Schechter and J. W. F. Valle, Phys. Rev. D **25**, 774 (1982).
[42] R. N. Mohapatra and J. W. F. Valle, Phys. Rev. D **34**, 1642 (1986).
[43] F. Bazzocchi, D. G. Cerdeno, C. Munoz, and J. W. F. Valle, arXiv:0907.1262.
[44] M. Malinsky, J. C. Romao, and J. W. F. Valle, Phys. Rev. Lett. **95**, 161801 (2005).
[45] K. S. Babu, Phys. Lett. B **203**, 132 (1988).
[46] A. Zee, Phys. Lett. **93B**, 389 (1980).
[47] D. Aristizabal Sierra, M. Hirsch, and S. G. Kovalenko, Phys. Rev. D **77**, 055011 (2008).
[48] C. Pena-Garay and A. Serenelli, arXiv:0811.2424.
[49] C. Biggio, M. Blennow, and E. Fernandez-Martinez, arXiv:hep-ph/0603036.
[50] A. de Gouvea and J. Jenkins, Phys. Rev. D **74**, 033004 (2006).
[51] J. Barranco, O. G. Miranda, C. A. Moura, and J. W. F. Valle, Phys. Rev. D **73**, 113001 (2006).
[52] A. Bolanos, O. G. Miranda, A. Palazzo, M. A. Tortola, and J. W. F. Valle, Phys. Rev. D **79**, 113012 (2009).
[53] S. Davidson, C. Pena-Garay, N. Rius, and A. Santamaria, J. High Energy Phys. 03 (2003) 011.
[54] C. Biggio, M. Blennow, and E. Fernandez-Martinez, J. High Energy Phys. 03 (2009) 139.
[55] Z. Berezhiani and A. Rossi, Phys. Lett. B **535**, 207 (2002).
[56] T. Schwetz, M. Tortola, and J. W. F. Valle, New J. Phys. **10**, 113011 (2008).
[57] M. Apollonio *et al.* (CHOOZ Collaboration), Phys. Lett. B **466**, 415 (1999).
[58] T. Araki *et al.* (KamLAND Collaboration), Phys. Rev. Lett. **94**, 081801 (2005).
[59] M. Guzzo *et al.*, Nucl. Phys. **B629**, 479 (2002).
[60] Y. Takeuchi, J. Phys. Conf. Ser. **120**, 052008 (2008).
[61] J. Klein (SNO Collaboration), ''*TAUP 2009*,'' 2009.
[62] J. N. Bahcall, K. Kubodera, and S. Nozawa, Phys. Rev. D **38**, 1030 (1988).
[63] J. Dorenbosch *et al.* (CHARM Collaboration), Phys. Lett. B **180**, 303 (1986).
[64] K. Nakamura (KamLAND Collaboration), AIP Conf. Proc. **721**, 12 (2004).
[65] A. Friedland, C. Lunardini, and M. Maltoni, Phys. Rev. D **70**, 111301 (2004).